CHARGED PARTICLE MULTIPLICITY AND CORRELATIONS IN HEAVY ION COLLISIONS IN THE ATLAS EXPERIMENT*

Bartłomiej Żabiński

on behalf of the ATLAS Collaboration

The H. Niewodniczański Institute of Nuclear Physics, Polish Academy of Sciences
Radzikowskiego 152, 31-342 Kraków, Poland

(Received April 19, 2013)

Since the start of the Large Hadron Collider (LHC) the ATLAS experiment has collected data from $p+p$, Pb+Pb, and recently p+Pb collisions. In this paper, two topics from the heavy ion programme are presented: the study of multiplicity of produced charged particles in Pb+Pb collisions and analysis of two-particle correlations in p+Pb interactions. In the first case, the dependence of particle production on collision centrality is examined. The second study of p+Pb collisions reveals long-range pseudorapidity correlations. These correlations for particles with $|\Delta\eta| > 2$ are stronger for more central collisions. Subtraction of the recoil contribution, present in the most peripheral collisions, from correlations measured for more central events discloses a quadrupole-like modulation in the azimuthal angle.

DOI:10.5506/APhysPolB.44.1691
PACS numbers: 25.75.–q, 25.75.Ag

1. Introduction

Collisions of Pb+Pb at the LHC provide an opportunity to study strongly interacting matter (Quark-Gluon Plasma, QGP) at the highest temperature created in the laboratory. Measurements of the charged particle multiplicity as a function of centrality in ultra-relativistic nucleus–nucleus collisions provide information on the initially created system. They can be used to estimate energy density of the system created in collisions. Two-particle correlations in pseudorapidity and azimuthal angle differences, $\Delta\eta$ and $\Delta\phi$, are sensitive to collective effects originating from strong interactions in the

* Presented at the Cracow Epiphany Conference on the Physics After the First Phase of the LHC, Kraków, Poland, January 7–9, 2013.

QGP. In elementary $p+p$ collisions, a strong enhancement of correlations is present at $\Delta\varphi \sim \pi$ (due to momentum conservation effects) and at $\Delta\varphi \sim 0$ for small $\Delta\eta$ only (from jets and resonance decays). However, in $p+p$ events with very large multiplicities, the correlation at $\Delta\varphi \sim 0$ extends to large $\Delta\eta$ forming a ridge structure [1]. A similar correlation is observed in p+Pb collisions at the LHC [2–4]. This paper presents results of ATLAS measurements of the charged particle pseudorapidity distribution $dN_{\mathrm{ch}}/d\eta$ in Pb+Pb collisions at $\sqrt{s_{NN}} = 2.76$ TeV and two-particle correlations in p+Pb collisions at $\sqrt{s_{NN}} = 5.02$ TeV.

2. The ATLAS detector

The ATLAS detector [5] is installed in one of four points, where the collisions of beams take place at the LHC [6]. It consists of different detector systems, starting with the inner detector followed by calorimeters and then muon chambers. Together they comprise one of the largest detectors in the world. The detector has been designed to provide a full azimuthal coverage and to cover a pseudorapidity range from −4.9 to 4.9. In this paper, we describe these parts of the detector which are used in the presented analyses. For the measurement of charged particle density, the most important is the pixel detector [5] shown in Fig. 1, the innermost part of the inner detector. It consists of three layers in the barrel and six disks in the endcaps region. The pixel detector contains 1744 silicon modules with over 80 millions of pixels. At larger radii, the inner detector consists of silicon-microstrip sensors, the SemiConductor Tracker (SCT) [5]. The SCT detector includes four layers

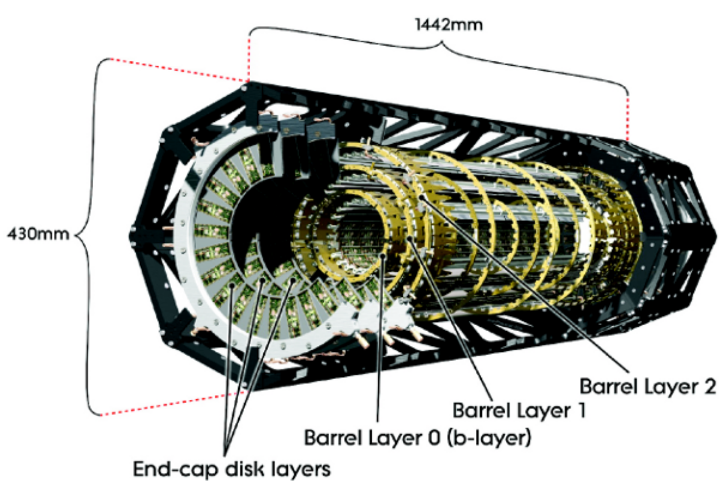

Fig. 1. The view of the pixel detector.

in the barrel region and eighteen disks in two endcaps. The outermost part of the inner detector is the Transition Radiation Tracker (TRT) [5] which contains up to 73 layers of straws in the barrel and 160 straw planes in endcaps. The other detector system is the liquid argon forward calorimeter (FCal) [5]. This detector covers the range $3.1 < |\eta| < 4.9$. For heavy ion physic studies, FCal is used to determine centrality of collisions.

3. Charged particle multiplicity in Pb+Pb collisions

The charged particle multiplicity is one of basic global characteristics of heavy ion collisions. The data used in this analysis were collected in 2010. Centrality of Pb+Pb collisions is defined by the impact parameter (the distance between the centres of colliding nuclei) and by the number of nucleons participating in the collision, $N_{\rm part}$. To determine the collision centrality, we use the total transverse energy deposited in FCal. Ten centrality classes are defined with the equal fraction of events in each centrality class [7]. The most central collisions have the largest transverse energy deposit in FCal.

Charged particle multiplicity was measured with three methods. The tracklet method [7, 8] finds a pair of hits (from different pixel layers) which are consistent with the reconstructed event vertex according to the condition

$$\Delta R \equiv \frac{1}{\sqrt{2}}\sqrt{\left(\frac{\Delta\eta}{\sigma_\eta(\eta)}\right)^2 + \left(\frac{\Delta\phi}{\sigma_\phi(\eta)}\right)^2} < 3\,, \tag{1}$$

where $\Delta\eta$ and $\Delta\phi$ represent deviations between the projected and measured hit positions in pseudorapidity and azimuthal angle, respectively, $\sigma_\eta(\eta)$ and $\sigma_\phi(\eta)$ characterize the pseudorapidity-dependent resolutions obtained from the Monte Carlo simulations. In addition to the two variants of the tracklet method (Method 1 and Method 2), pixel tracks obtained from the standard track reconstruction [9] were also used in the multiplicity analysis. The charged particle pseudorapidity distribution in most central Pb+Pb collisions is shown in Fig. 2 (left) [7]. Colour dots represent raw measurements from the three methods which are distinctly different (top plot). However, after applying efficiency and background corrections derived from Monte Carlo simulation [7], the three independent measurements agree within 7% (bottom plot). The right panel in Fig. 2 presents the corrected charged particle density as a function of pseudorapidity for eight centrality classes.

In the 0–10% of most central collisions, the charged particle density, $dN_{\rm ch}/d\eta|_{\eta=0}$ reaches $1479\pm10(\text{stat.})\pm63(\text{sys.})$, where $dN_{\rm ch}/d\eta|_{\eta=0}$ is averaged over $|\eta| < 0.5$. The number of produced charged particles increases with centrality, while its pseudorapidity dependence is relatively weak.

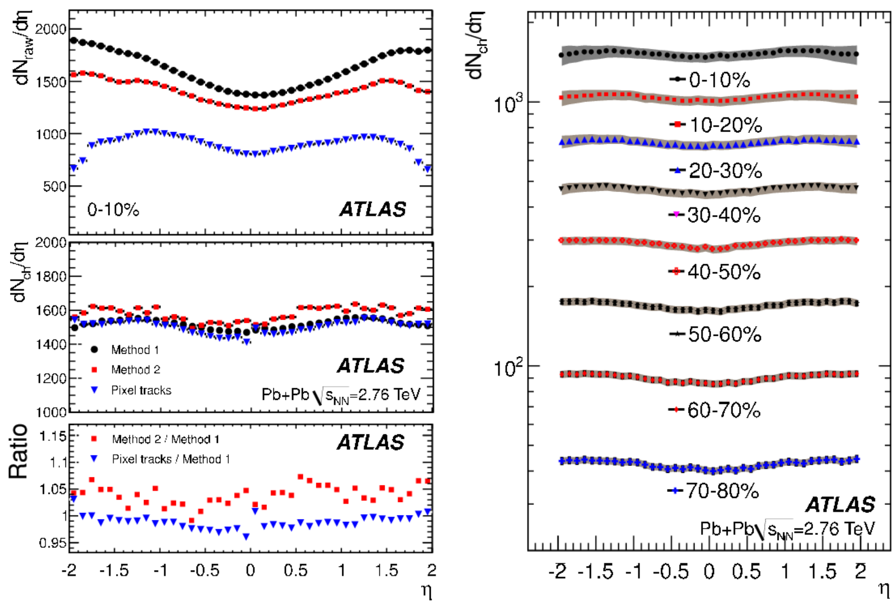

Fig. 2. Left: Pseudorapidity dependence of the uncorrected charged particle density, $dN_{\rm raw}/d\eta$ in Pb+Pb collisions for the 0–10% centrality interval (top plot). In the middle plot, the same dependence is shown for the corrected charged particle density. In both plots, black points represent the tracklet Method 1, red squares the tracklet Method 2, and blue triangles the pixel track method. The bottom plot shows the ratio of these measurements. Right: Pseudorapidity dependence of the charged particle density obtained from the tracklet Method 1 for eight centrality classes [7].

Using the Glauber Monte Carlo model [10], it is possible to estimate the number of nucleons participating in collisions, $N_{\rm part}$, for each centrality class. Centrality dependence of the charged particle density, normalized to the number of participant nucleon pairs, is shown in Fig. 3. The ATLAS measurements are consistent with ALICE results [11], and with RHIC [12–15] and PHOBOS [14] measurements after rescaling the RHIC results by a factor of 2.15. A similar monotonic increase of $dN_{\rm ch}/d\eta|_{\eta=0}/(\langle N_{\rm part}\rangle/2)$ with $\langle N_{\rm part}\rangle$ is observed at different collision energies.

Energy dependence of the charged particle multiplicity, per one pair of participants, $dN_{\rm ch}/d\eta|_{\eta=0}/(\langle N_{\rm part}\rangle/2)$ is presented in Fig. 4. The results from the LHC experiments (ATLAS [7], ALICE [11] and CMS [16]) obtained at $|\eta| < 0.5$ for the 0–5% centrality interval are compared to those for other collision systems and different energies. The results from all LHC experiments are consistent and indicate a faster multiplicity increase with $\sqrt{s_{NN}}$ than expected from a simple extrapolation of results at lower energies.

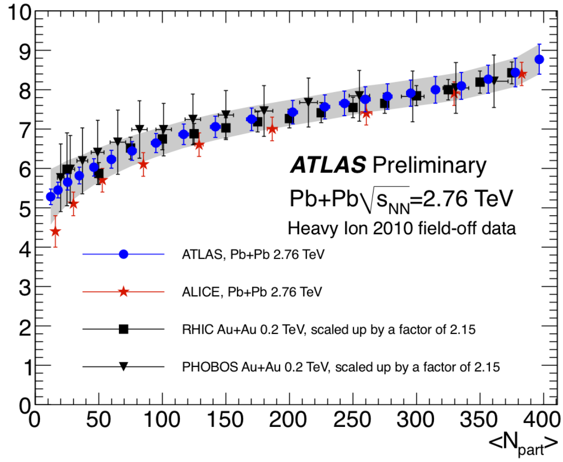

Fig. 3. Charged particle multiplicity normalized to a pair of nucleons participating in collisions, as a function of N_{part} [7]. Error bars represent combined statistical and systematic uncertainties, whereas the shaded band indicates the total systematic uncertainty. The RHIC results are scaled by a factor of 2.15 to allow for the comparison with the ATLAS and ALICE results.

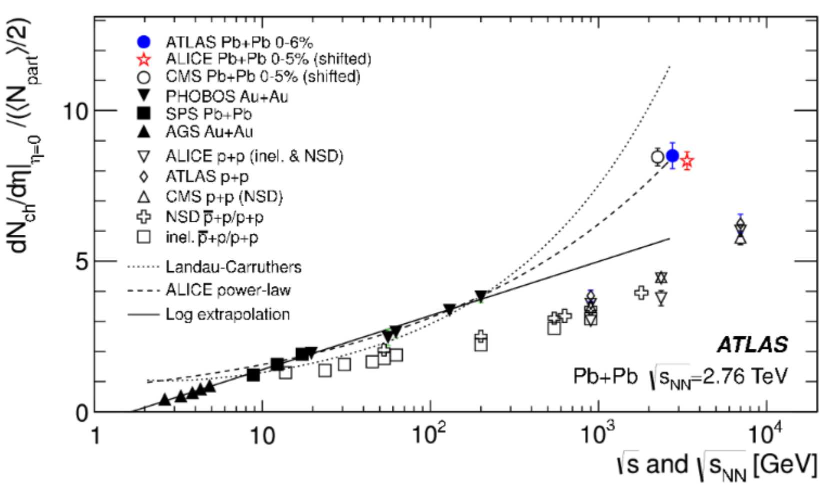

Fig. 4. Energy dependence of the charged particle density per a pair of participating nucleons $dN_{\mathrm{ch}}/d\eta|_{\eta=0}/(\langle N_{\mathrm{part}}\rangle/2)$ from a variety of measurements in $p+p$, $\bar{p}+p$ and central $A+A$ collisions, including the ATLAS results for 0–6% centrality interval, and ALICE and CMS results for 0–5% centrality interval. The curves show different parametrization of the $\sqrt{s_{NN}}$ dependence in $A+A$ collisions as described in the legend [7].

4. Two-particle correlations in p+Pb collisions

In September 2012, the LHC delivered p+Pb collisions at 5.02 TeV nucleon–nucleon centre of mass energy. The data from this first run were used in the analysis of two-particle correlations [4]. Centrality of p+Pb collisions is defined using the transverse energy deposited in FCal. However, due to the asymmetry of colliding beams, the total transverse energy measured in FCal only on the Pb fragmentation side ($3.1 < \eta < 4.9$) is used. The distribution of $\sum E_{\mathrm{T}}^{\mathrm{Pb}}$ in FCal for minimum bias p+Pb events is shown in Fig. 5.

These events are divided into twelve centrality intervals, as indicated in Fig. 5. In the analysis, two larger intervals are also used: $\sum E_{\mathrm{T}}^{\mathrm{Pb}} > 80$ GeV referred to as central and $\sum E_{\mathrm{T}}^{\mathrm{Pb}} < 20$ GeV referred to as peripheral. In the ALICE [3] and CMS [2] study of p+Pb collisions, the charged particle multiplicity is used to define centrality intervals. Both measures of centrality are similar, as the FCal $\sum E_{\mathrm{T}}^{\mathrm{Pb}}$ and the number of reconstructed charged particles are strongly correlated (see Fig. 6). Centrality defined by FCal signal, recorded in a phase space region separated from the region covered by charged particle measurements, does not introduce systematic biases in analyses involving charged particles. Such systematic biases are present when the charged particle multiplicity is used to define centrality of the collision.

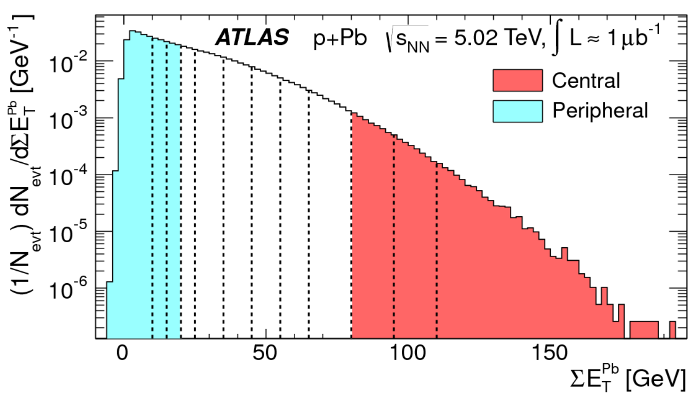

Fig. 5. Distribution of transverse energy registered in FCal detector at the lead fragmentation side, $\sum E_{\mathrm{T}}^{\mathrm{Pb}}$, for p+Pb events [4]. Vertical lines indicate different centrality intervals. Shaded bands indicate peripheral and central events, see the text for details.

The two-particle correlation function (2PC) is calculated using Eq. (2),

$$C(\Delta\phi, \Delta\eta) = \frac{S(\Delta\phi, \Delta\eta)}{B(\Delta\phi, \Delta\eta)}\,, \tag{2}$$

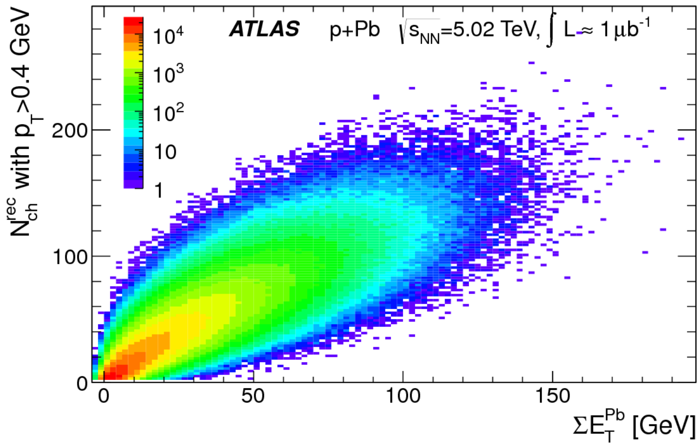

Fig. 6. Correlation between the number of reconstructed charged particles and the energy registered in FCal detector, $\sum E_{\mathrm{T}}^{\mathrm{Pb}}$ [17].

where S (B) is the distribution of pairs constructed from the same event (from mixed events), $\Delta\phi = \phi_a - \phi_b$ and $\Delta\eta = \eta_a - \eta_b$, and labels a, b denote particles forming a pair. The following analysis is restricted to charged particle pairs with $2 < |\Delta\eta| < 5$.

The two-dimensional correlation function is shown in Fig. 7 for peripheral and central p+Pb collisions (top panels). For peripheral events, the correlation function shows a sharp peak at $(\Delta\phi, \Delta\eta) = (0, 0)$ due to pairs originating from resonance decays and from jets, and a broad structure at $\Delta\phi \sim \pi$ due to dijets and momentum conservation. In central events, the correlation function reveals a long-range structure in pseudorapidity (ridge-like) at $\Delta\phi \sim 0$ (the near-side). On the away-side ($\Delta\phi \sim \pi$), the distribution is broader than in peripheral collisions, indicating also a presence of long-range pseudorapidity correlations. The strength of these long-range correlation is defined as the per-trigger yield, $Y(\Delta\phi)$

$$Y(\Delta\phi) = \left(\frac{\int B(\Delta\phi) d\Delta\phi}{\pi N_a}\right) C(\Delta\phi) - b_{\mathrm{ZYAM}}\,, \tag{3}$$

where N_a is the total number of trigger particles and b_{ZYAM} is a pedestal (see [4] for details).

The $Y(\Delta\phi)$ distributions for central and peripheral events are shown in Fig. 7 (c). The yield for central events has peaks in the near-side and the away-side and the peak in the away-side has a larger magnitude. In contrast, the yield for peripheral events has a maximum in the away-side only and minimum in the near-side. In order to study correlations quantitatively,

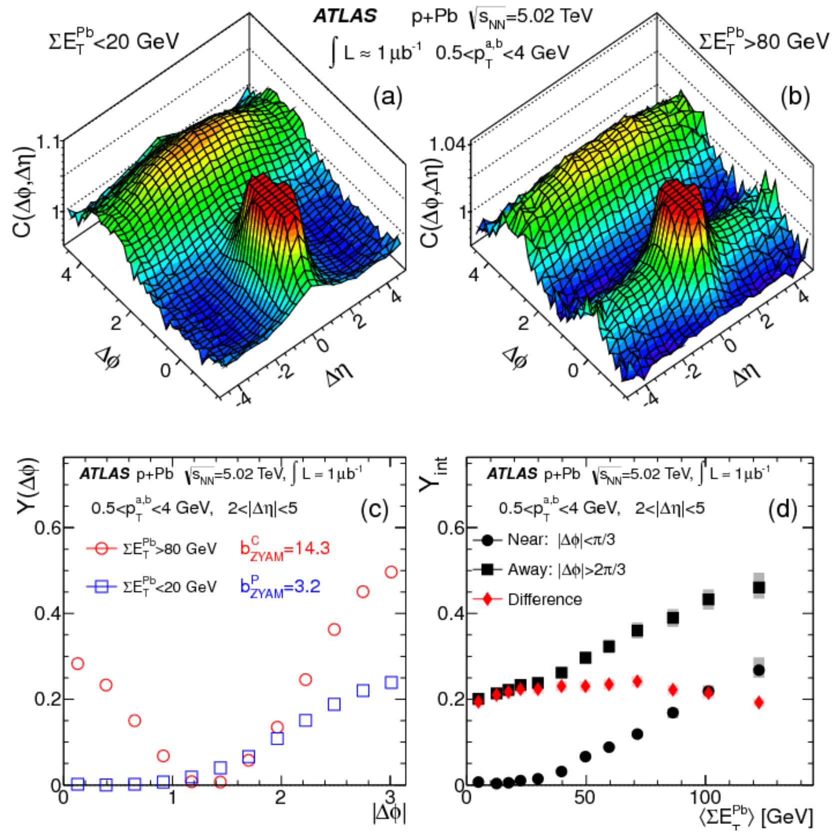

Fig. 7. Top: 2-D correlation function for (a) peripheral and (b) central p+Pb events. Bottom: (c) The per-trigger yield as a function of $|\Delta\phi|$ for central (red circles) and peripheral (blue squares) collisions, (d) integrated per-trigger yield as a function of event centrality [4].

we integrate the yield in the near-side ($|\Delta\phi| < \pi/3$) and the away-side ($|\Delta\phi| > 2\pi/3$) and plot the yields as a function of $\sum E_{\mathrm{T}}^{\mathrm{Pb}}$ in Fig. 7 (d). The difference between these two yields is approximately constant, while the increase of yields with $\sum E_{\mathrm{T}}^{\mathrm{Pb}}$ is similar on the near-side and away-side. The distributions of $Y(\Delta\phi)$ for central and peripheral events are studied in four p_{T}^{a} intervals covering the full $0.5 < p_{\mathrm{T}}^{b} < 4$ GeV range (see Fig. 8). The difference between central and peripheral yields is also shown and overlaid with quadrupole functions $a_0 + 2a_2 \cos 2\Delta\phi$, where $a_0 = \langle \Delta Y(\Delta\phi)\rangle$ and $a_2 = \langle \Delta Y(\Delta\phi) \cos 2\Delta\phi\rangle$. The long-range component of the two-particle correlations can be thus approximately described by a momentum conservation (recoil) contribution plus a $\Delta\phi$-symmetric quadrupole component.

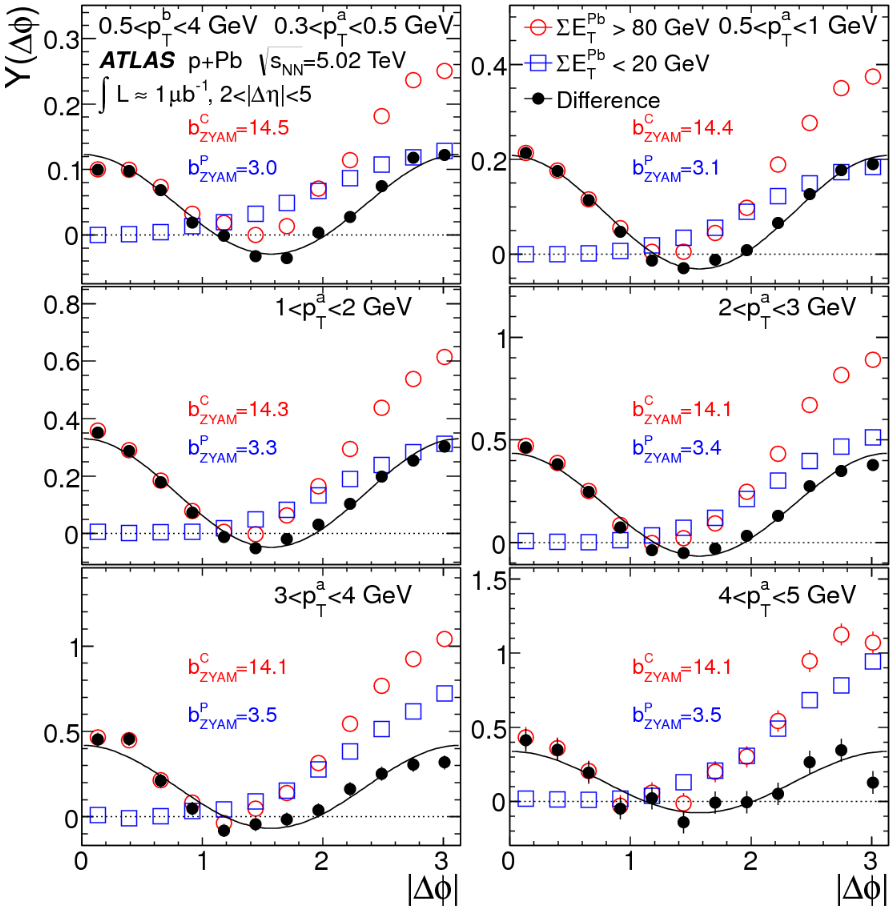

Fig. 8. Distributions of per-trigger yield in the peripheral (circle) and central (square) events and their difference (black dots) for different p_{T}^{a} ranges. The pedestal levels are indicated on each panel separately for peripheral ($b_{\mathrm{ZYAM}}^{\mathrm{P}}$) and central ($b_{\mathrm{ZYAM}}^{\mathrm{c}}$) events [4]. See the text for explanation of the shown functions.

The magnitude of the integrated per-trigger yield on the near-side and away-side ($|\Delta\phi| < \pi/3$ and $|\Delta\phi| > 2\pi/3$, respectively) and their difference in central and peripheral collisions, ΔY_{int} is shown in Fig. 9 as a function of p_{T}^{a}. The differences have a similar $p_{\mathrm{T}}^{\mathrm{a}}$ dependence on the near-side and away-side, they rise with increasing p_{T}^{a} up to ~ 3 GeV and then become constant or even slightly decrease. A similar dependence is observed for ridge-like correlations in Pb+Pb collisions at approximately the same p_{T} [18, 19].

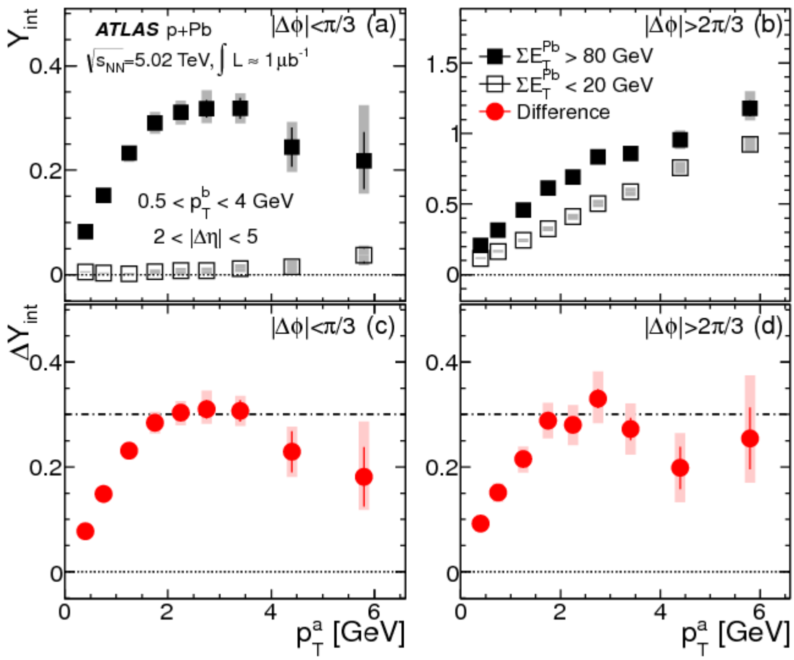

Fig. 9. Integrated per-trigger yield as a function of p_{T}^{a} for central and peripheral events on the near-side (a) and away-side (b) and their differences in (c) and (d), respectively [4].

Finally, to quantify the strength of the $\cos(2\Delta\phi)$ modulation of $\Delta Y(\Delta\phi)$, the amplitude c_2 is calculated as

$$c_2 \equiv \frac{a_2}{b_{\mathrm{ZYAM}}^{\mathrm{c}} + a_0} \,. \tag{4}$$

In Fig. 10, the parameter c_2 is plotted as a function of the trigger particle transverse momentum. The c_2 parameter can be converted to the average quadrupole modulation of event-by-event single particle ϕ distribution,

$$s_2(p_{\mathrm{T}}^{a}) \equiv \frac{c_2\left(p_{\mathrm{T}}^{a}, p_{\mathrm{T}}^{b}\right)}{\sqrt{5.4 \pm 0.1 \times 10^{-3}}} \,, \tag{5}$$

where $\sqrt{5.4 \pm 0.1 \times 10^{-3}}$ is derived from Eq. (4) using a_2 obtained from the difference between the central and peripheral data shown in Fig. 7 (c). Values of s_2 parameter are given on the vertical axis on the right side of Fig. 10. The magnitude of s_2 and its transverse momentum dependence is similar to that observed for the elliptic flow Fourier coefficient measured in Pb+Pb collisions [20].

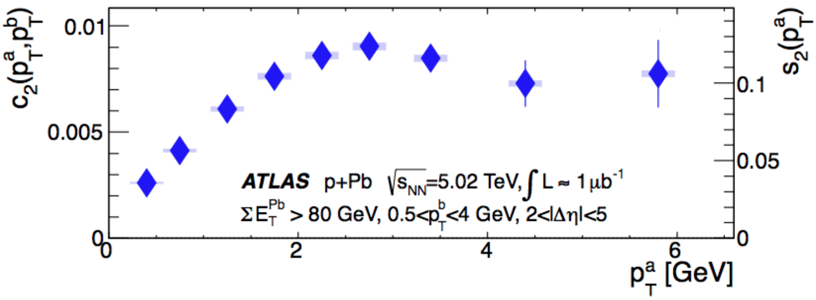

Fig. 10. The p_{T}^a dependence of c_2 (left axis) and s_2 (right axis). The error bars represent statistical errors and shaded boxes represent systematics uncertainties [4].

5. Summary

The ATLAS experiment has measured charged particle multiplicity in a wide range of four pseudorapidity units, and for transverse momenta starting from 30 MeV. The charged particle density, $dN_{\mathrm{ch}}/d\eta$, normalized by $\langle N_{\mathrm{part}}\rangle/2$ is found to be similar to that measured at lower energy by RHIC experiments, when the overall increase with energy by a factor of 2.15 is assumed. In p+Pb collisions, two-particle correlations have been studied with a focus on the long-range pseudorapidity correlations. Strong long-range ridge-like correlations are observed both on the near-side and away-side. After subtracting the contribution expected from momentum conservation effects, the resultant $\Delta\phi$ correlation shows $\cos(2\Delta\phi)$ modulation with the amplitude and p_{T} dependence similar to modulations observed in Pb+Pb collisions.

This work was supported in part by the Polish National Science Center grant No. DEC-2011/03/B/ST2/02631. This research was supported in part by PL-Grid Infrastructure.

REFERENCES

[1] CMS Collaboration, *J. High Energy Phys.* **1009**, 091 (2010).
[2] CMS Collaboration, *Phys. Lett.* **B718**, 795 (2013).
[3] ALICE Collaboration, *Phys. Lett.* **B719**, 29 (2013).
[4] ATLAS Collaboration, `arXiv:1212.5198 [hep-ex]`, submitted to *Phys. Rev. Lett.*
[5] ATLAS Collaboration, *JINST* **3**, S08003 (2008).
[6] L. Evans, P. Bryant (Eds.), *JINST* **3**, S08001 (2008).

[7] ATLAS Collaboration, *Phys. Lett.* **B710**, 363 (2012).
[8] B. Żabiński, *Acta Phys. Pol. B* **42**, 1729 (2011).
[9] T. Cornelissen *et al.*, *J. Phys. Conf. Ser.* **119**, 032014 (2008).
[10] M.L. Miller, K. Reygers, S.J. Sanders, P. Steinberg, *Annu. Rev. Nucl. Part. Sci.* **57**, 205 (2007).
[11] ALICE Collaboration, *Phys. Rev. Lett.* **106**, 032301 (2011).
[12] PHENIX Collaboration, *Phys. Rev.* **C71**, 034908 (2005) [*Erratum ibid.*, **C71**, 049901 (2005)].
[13] BRAHMS Collaboration, *Phys. Rev. Lett.* **88**, 202301 (2002).
[14] PHOBOS Collaboration, *Phys. Rev.* **C65**, 061901 (2002).
[15] STAR Collaboration, *Phys. Rev.* **C70**, 054907 (2004).
[16] CMS Collaboration, *J. High Energy Phys.* **1108**, 141 (2011).
[17] ATLAS Collaboration, `https://atlas.web.cern.ch/Atlas/GROUPS/PHYSICS/ PAPERS/HION-2012-13/`
[18] CMS Collaboration, *Eur. Phys. Rev. J.* **C72**, 2012 (2012).
[19] ATLAS Collaboration, *Phys. Rev.* **C86**, 014907 (2012).
[20] ATLAS Collaboration, *Phys. Lett.* **B707**, 330 (2012).